Summer Internship Report on

Quantitative Assessment of Electrode Array Configurations for subterranean cavity detection within coal mines region using 2D ERT Forward and Inverse modeling

Duration: June 25TH, 2023 – August 11TH, 2023

UNDER THE MENTORSHIP OF

Dr. ABHAY KUMAR BHARTI, SCIENTIST

SUBMITTED TO

CSIR – CENTRAL INSTITUTE OF MINING AND FUELING RESEARCH, DHANBAD

SUBMITTED BY

SUMIT KUMAR MOHAPATRA

22MC0098

M.SC TECH APPLIED GEOPHYSICS, IIT ISM, DHANBAD

DECLARATION

I hereby declare that the one-month vocational training report entitled "**Quantitative Assessment of Electrode Array Configurations for subterranean cavity detection within coal mines region using 2D ERT Forward and Inverse Modeling**" has been carried out under the guidance of **Dr. Abhay Kumar Bharti, Scientist**, CENTRAL INSTITUTE OF MINING AND FUEL RESEARCH, Dhanbad. This training report has been not submitted elsewhere.

Place: CSIR-CIMFR, Dhanbad **SUMIT KUMAR MOHAPATRA**

Date- 11/ 08/ 2023

ACKNOWLEDGEMENT

In this moment of accomplishment, I am humbled and grateful for the guidance and support that have shaped my journey. I extend my sincere thanks to **CSIR – Central Institute of Mining and Fuel Research, Dhanbad**, for their generous provision of resources and assistance during the course of this training.

I am indebted to **Dr. Abhay Kumar Bharti**, a remarkable Scientist at CSIR-CIMFR, for his invaluable mentorship. His insights, encouragement, and scholarly direction have been pivotal in navigating the complexities of this project.

I would also like to extend my appreciation to the academic leadership at **IIT (ISM), Dhanbad,** including **Prof. S. K. Pal**, **HOD of the Department of Applied Geophysics**, and **Prof. S. D. Gupta**, **Associate Professor & DPGC**, for their instrumental role in facilitating this learning opportunity.

Last but never least, my heartfelt gratitude goes to my parents, whose unwavering support and motivation have been the cornerstone of my achievements.

SUMIT KUMAR MOHAPATRA

CERTIFICATE

This is to certify that **Mr. SUMIT KUMAR MOHAPATRA** of the **INDIAN INSTITUTE of TECHNOLOGY (INDIAN SCHOOL of MINES), Dhanbad** has undergone summer training from June 25, 2023, to August 11, 2023, at **CSIR-CIMFR (Central Institute of Mining and Fuel Research), Dhanbad** in the Research Group of Mine Planning and Economics Subsidence and Surveying has made the project report under my guidance.

PROJECT GUIDE:

Dr. Abhay Kumar Bharti, Scientist **Signature with date**

Department of Mine Planning and Economics,

CSIR-CIMFR, Dhanbad-826006

ABSTRACT

This project delves into the "Quantitative Assessment of Electrode Array Configurations for subterranean cavity detection within coal mines region using 2D ERT Forward and Inverse modeling." The primary objective of this study is to discern the most effective electrode array configuration for subterranean cavity detection in coal mine regions through the utilization of 2D Electrical Resistivity Tomography (ERT) techniques.

The project's core focus revolves around the meticulous evaluation and selection of an optimal electrode array configuration that yields exceptional performance in both forward and inversion results. To accurately replicate real-world field scenarios, a controlled level of complexity was introduced by incorporating a 5% Gaussian noise into the data. The investigation incorporated three distinct survey electrode configurations: Wenner-Schlumberger, Pole-Dipole, and Dipole-Dipole arrays.

To elevate the resolution of the findings, the research culminated in the application of Data Level Synthesization (DLS). This advanced technique amalgamated the forward model outputs from each array configuration into a unified file prior to the inversion process. By leveraging this approach, the study aimed to refine the accuracy and reliability of the detected subterranean cavity features.

The results of this research are anticipated to offer significant insights into optimal electrode array selection for subterranean cavity detection within coal mines. This endeavour contributes to the advancement of geophysical survey methodologies and holds the potential to enhance the safety and efficiency of mining operations by enabling more precise detection of underground voids.

TABLE OF CONTENTS

INTRODUCTION

The covert existence of subsurface cavities poses a multifaceted threat to public safety, infrastructure stability, and environmental integrity. The critical need to avert potential disasters arising from these hidden voids underscores the urgency of precise detection. This research paper is dedicated to advancing subsurface imaging using Electrical Resistivity Tomography (ERT), focusing on bridging the gap between accurate detection and cost-effectiveness.

This project is focused on the recognition of the 2D ERT survey as a foundational solution for subsurface cavity detection. The efficiency and economy of this method, coupled with minimal manpower requirements, make it an ideal initial approach Compared to other geophysical imaging techniques, resistivity tomography is faster, cheaper, covers larger areas, provides clear details, reaches deeper depths, and is easy to interpret. Additionally, the research delves into the synthesis of multiple geoelectrical arrays, enhancing data reliability and predictive capabilities. Our work primarily revolves around evaluating the efficacy of different electrode configuration arrays based on their sensitivity and the subsurface imaging they produce using pseudo-section techniques. This preliminary assessment before conducting the field survey is achieved through forward modeling with the aid of RES2DMOD software, coupled with inversion using RES2DINV software.

This research paper focuses on enhancing subsurface imaging using Electrical Resistivity Tomography (ERT) with three primary goals:

a. Utilizing multiple geoelectrical resistivity arrays to compensate for individual weaknesses found in common arrays and determine suitable array for field data acquisition

b. Introducing the Data Levels Synthesization (DLS) method to effectively merge data from two different arrays, enhancing the reliability of subsurface parameter predictions.

c. Evaluating the performance of the res2dinv software under real field conditions by incrementally enhancing the Gaussian noise value in the model.

1. THEORY

1.1. ELECTRICAL PROPERTIES OF EARTH

The electric current propagates through subsurface rocks and minerals in three ways: electronic(ohmic), electrolytic, and dielectric conduction. In electronic conduction, the movement of free electrons in an externally applied field takes place as in metals.

But the flow of current through subsurface rocks would be merely impossible due to their high resistivities if it were not for the fact that they are porous. These pore spaces are filled with fluids, as a result, the rocks are electrolytic conductors. In electrolytic conduction, the propagation of current is the result of ionic conduction- by the molecules having an excess or deficiency of electrons. The conductivity of such partially or fully saturated rocks depends upon the porosity of the rock, fluid saturation, cement type, and fluid resistivity. The resistivity of such rocks can be found through empirical relationship as proposed by Archie in 1942:

$$R = \frac{aR_\omega}{\phi^m S_\omega^n}$$

Where a= tortuosity factor, R_ω = Fluid resistivity, ϕ = Porosity, S = Water Saturation, m=cementation factor, n = saturation exponent

Conductive materials, like water-saturated or mineralized zones, have low resistivity, while resistive materials, such as solid rocks or dry soil, have high resistivity.

1.2. VERTICAL ELECTRICAL SOUNDING

The method involves injecting an electric current into the ground through a pair of electrodes and measuring the resulting voltage potential using another pair of electrodes. By varying the separation between the electrodes and analysing the current-voltage relationship, the apparent resistivity of subsurface layers at different depths can be determined.

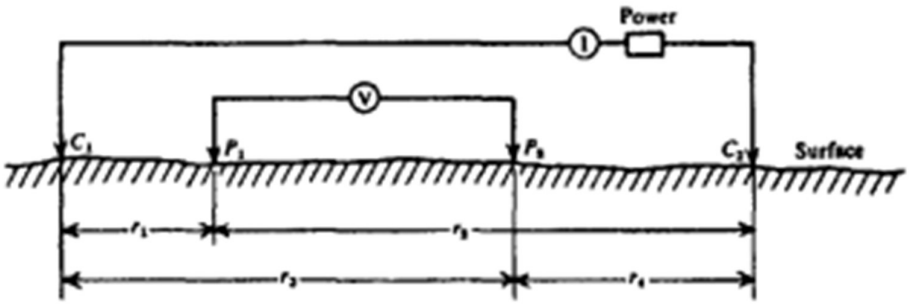

Figure 1. Two current electrodes and two potential electrodes on the surface of homogenous isotropic ground of resistivity ρ, I=Current flowing through the subsurface.

The potential due to C1 at P1 is:

$$v_1 = -\frac{I\rho}{2\pi} r_1$$

The potential due to C2 at P1 is:

$$v_2 = -\frac{I\rho}{2\pi} r_2$$

The net potential at P1 is:

$$v_1 + v_2 = \frac{I\rho}{2\pi}\left(\frac{1}{r_1} - \frac{1}{r_2}\right)$$

Similarly, the net potential at P2 is:

$$v_3 + v_4 = \frac{I\rho}{2\pi}\left(\frac{1}{r_3} - \frac{1}{r_4}\right)$$

The measured potential difference (Δv) between P1 and P2 is:

$$\boxed{\Delta v = \frac{I\rho}{2\pi}\left\{\left(\frac{1}{r_1} - \frac{1}{r_2}\right) - \left(\frac{1}{r_3} - \frac{1}{r_4}\right)\right\}}$$

The VES technique significantly enhances resistivity surveys by enabling the acquisition of subsurface images from greater depths.

1.3. 2D ELECTRICAL RESISTIVITY TOMOGRAPHY METHOD

The two-dimensional (2-D) ERT method is amongst the most popular non-destructive and non-invasive technique geophysical methods used for subsurface imaging in environmental and engineering research. In ERT, a set of electrodes (**Current electrodes C1 and C2**) is placed on the ground surface, and a small electrical current is injected into the ground through these electrodes. The resulting voltage distribution is then measured by another set of electrodes (**Potential electrodes P1 and P2**). It is based on an old technique called Pseudosection. This technique had been used until the early 1990s, and it maps the subsurface in a 2D cross-section using Vertical Electrical Sounding (VES) and Constant Separation Traverse (CST) techniques. It captures the lateral and vertical changes of subsurface apparent resistivity at the same. In the forward modeling approach, we can recreate the real field scenario by generating the apparent resistivity data based on the current sensitivity function of the electrode array and the model and the model parameter (true resistivity).

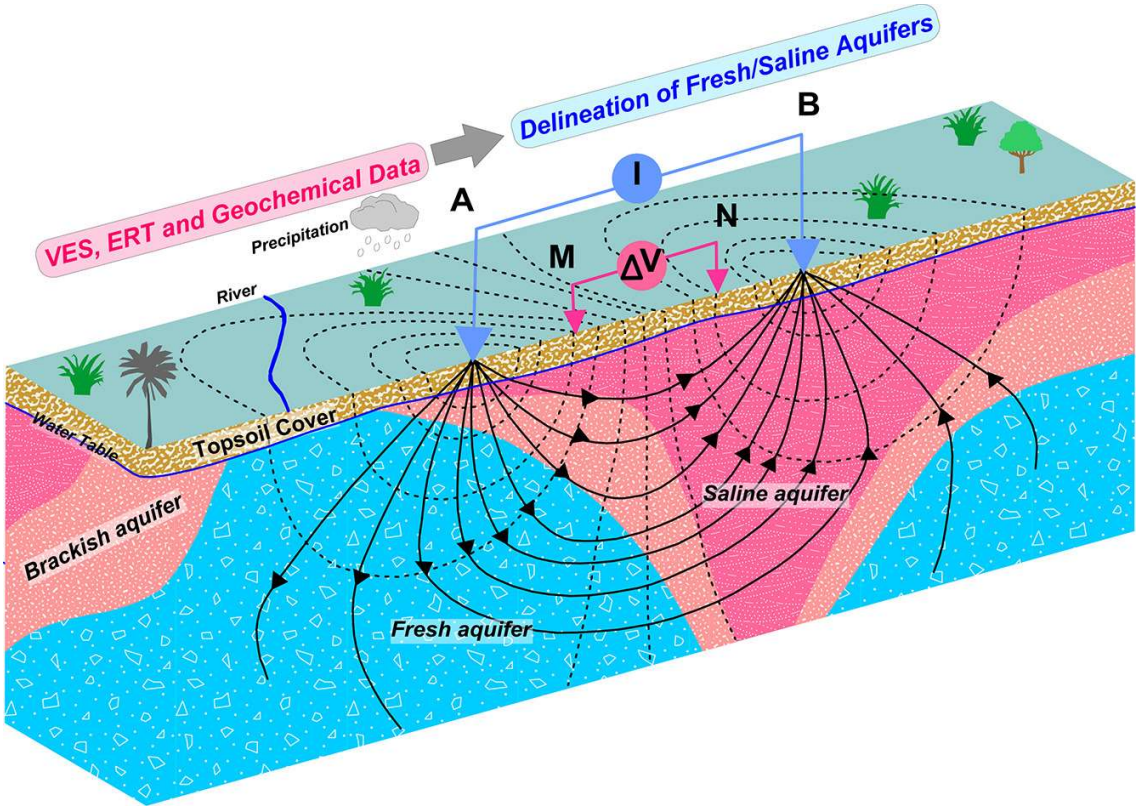

Figure 2. Illustration of the behaviors of the streamlines and the equipotentials during a VES survey of an aquifer (Hasan et al., 2019)

There are many choices of geoelectrical arrays that can be applied during the field survey based on the objectives of the research study. In this research paper arrays used were Wenner-Schlumberger, dipole–dipole, and pole-dipole arrays. Various researchers have made comparisons among these common arrays in terms of their depth of investigations (Roy and Apparao, 1971; Barker, 1989; Oldenburg and Li, 1999; Szalai et al., 2009), accuracy and resolution of the inverted resistivity data (Sasaki, 1992; Beard and Tripp, 1995; Dahlin and Zhou, 2004).

1.2. ELECTRODE ARRAY CONFIGURATIONS

One of the problems of resistivity investigations is the choice of a suitable electrode configuration that will provide the best response to the buried caves in the subsurface (ZHOU and GREENHALGH 2000; ZHOU and DAHLIN 2003). Several electrode arrays have been used in resistivity investigations, including Wenner, Wenner-Schlumberger, dipole-dipole, pole-pole, and pole-dipole arrays (DAHLIN 1996; CHAMBERS et al. 1999; STORZ et al. 2000) and hundreds more different configurations.

Each electrode array has its advantages and limitations regarding field operations and interpretation capabilities. The depth of investigations (ROY and APPARAO 1971; BARKER 1989; OLDENBURG and LI 1999; SZALAI and SZARKA 2008), sensitivity to horizontal or vertical variations (LOKE et al. 2003; DAHLIN and ZHOU 2004), and signal strength (LOKE 2001; SEATON and BURBEY 2002; DAHLIN and ZHOU 2004; CANDANSAYAR 2008) are the important factors, which determine the resolving capabilities of each array for various subsurface targets. In addition, the geological structures to be mapped, heterogeneities of the subsurface, sensitivity of the arrays to vertical and lateral variations in the resistivity of the subsurface, and horizontal data coverage should be considered before embarking on field surveys.

1.2.1. POLE–DIPOLE ARRAY

One of the current electrodes (i.e. C2) is fixed at a great distance from the other three, all of which can have various spacings. The two potential electrodes P1 and P2 are used to map out the subsurface. This arrangement is equivalent to a half-Schlumberger array. Because the electrode is remote, it is not necessary to have it in line with the other three. This permits lateral exploration on radial lines from a fixed position of C1 by moving one or both potential electrodes, a particularly convenient method for resistivity mapping in the vicinity of a

conductor of a limited extent. This electrode arrangement is effectively the same as the lateral spread used in well logging.

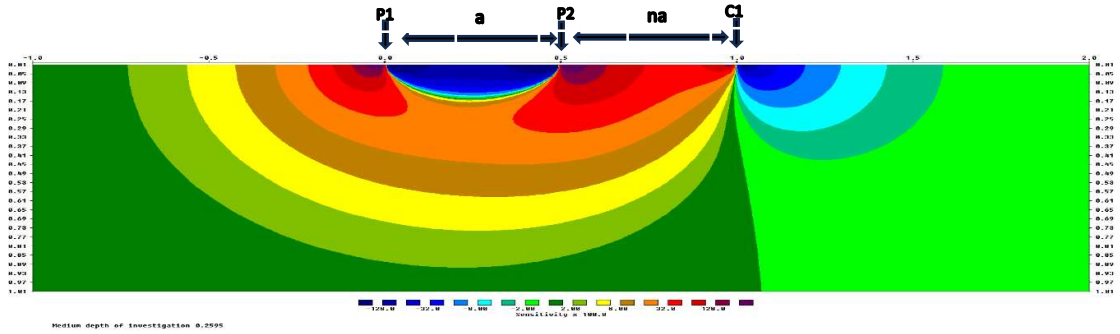

Figure 3. Illustration of the Pole-Dipole Configuration Array

1.2.2. DIPOLE-DIPOLE ARRAY

The best array to measure apparent resistivity in complex structures is the dipole-dipole array. The dipole-dipole array, consisting of a current electrode pair and a potential electrode pair, was originally used for mineral exploration with the induced polarization (IP) method. In order to get an idea of the earth's cross-section, the result of a survey is plotted in a so-called pseudo-section, where the apparent resistivity data is plotted at the midpoint between the two dipoles and at a depth of 18% of the dipole-to-dipole separation. The values are then

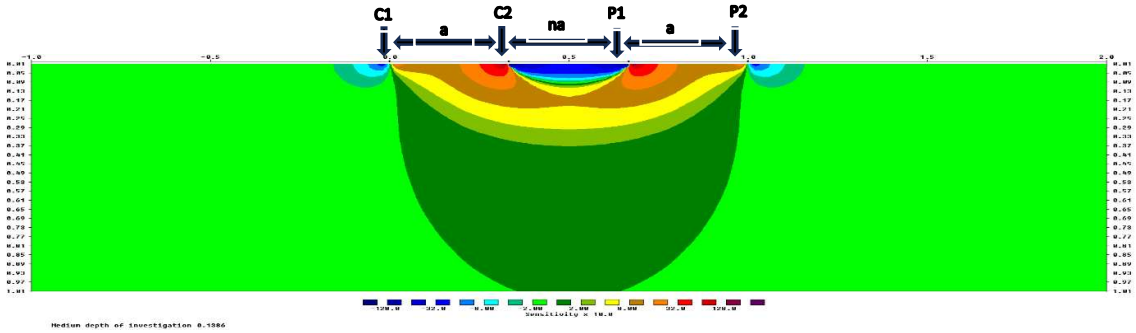

Figure 4. Illustration of the Pole-Dipole Configuration Array

contoured and colorized to represent a rough image of the subsurface. It is the job of modern inversion software to recalculate all these apparent resistivity values to "true" resistivity so that a realistic image of the ground can be created.

When compared to the Wenner array, which provides a big picture, the dipole-dipole array provides great detail. The disadvantage is that it doesn't reach very

deep as the receiving dipole will lose the signal if they are placed too far from the transmitting dipole.

1.2.3. WENNER-SCHLUMBERGER ARRAY

In the Wenner-Schlumberger array, the electrode position is as same the Wenner Alpha method, but the distance between the electrode current and potential electrodes is "n" times the distance of the two potential electrodes This configuration is shown in Figure, the geometry factor, $k=\pi n(n + 1)a$. This configuration also detects the greater concentration of high resistivity below the M-N electrodes. That implies the Wenner-Schlumberger configuration is sensitive to changes in resistivity horizontally and vertically. According to Loke (2000), in areas that have complex geological conditions, this method will be more promising than the configuration of Wenner Alpha and Dipole-dipole. Depth investigation of this configuration is 10 % deeper than the Wenner configuration with the same distance between A-B electrodes.

The signal strength is higher than the Wenner configuration but higher than the Dipole-dipole configuration Wenner-Schlumberger method is also able to cover Wenner configuration weaknesses such as bad horizontal coverage, although it is not better than the Dipole-dipole configuration.

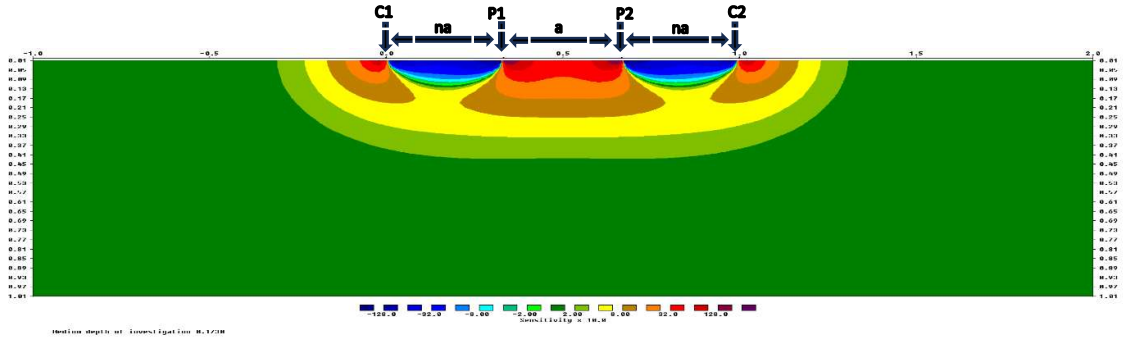

Figure 5. Illustration of the Pole-Dipole Configuration Array

2. METHODOLOGY

Our goal is to test the efficiency of different electrode configurations in subsurface cavities detection before carrying out a field survey. Thus, we started with creating subsurface models in Res2dmod software based on the geological

information found in subsurface caving or water-logged zones in coal seams. We created three subsurface models, all featuring identical geological formations. However, each model simulated a different real-field scenario.

Wenner-Schlumberger array, Pole-Dipole array, and Dipole-Dipole electrode array configurations were chosen. Using the initial subsurface model and the chosen array configurations, we performed forward modeling in Res2dmod to calculate the synthetic or measured apparent resistivity pseudo section. The calculated pseudo section represents what would be observed if the initial model perfectly matched the true subsurface resistivity distribution.

The forward-modeled apparent resistivity pseudo section for each array configuration was then saved in a DAT file, which contained the synthetic data. 5% Gaussian noise was added to each synthetic dataset to reflect the real field scenario. This DAT file was then used as input for the Res2DInv software.

In the Res2DInv software, the inversion process begins with the synthetic apparent resistivity pseudo section saved in dat format. The inversion starts with an initial guess model. The inversion model divides the subsurface into a number of rectangular cells surrounding pseudo-section data points and assigns model parameters (i.e., resistivity) to each cell based on an optimization algorithm.

An objective function and a sensitivity matrix are defined. The objective function includes a data misfit term (measuring the difference between the observed and computed pseudo sections) and a regularization term (to control model smoothness). The sensitivity matrix (also known as the Jacobian matrix) relates the changes in the model parameters (resistivity values) to the changes in the calculated apparent resistivity values. The sensitivity matrix is obtained through numerical differentiation.

Based on the initial guess model, a computed apparent resistivity pseudo section is generated through finite difference modeling. Using the objective function and the sensitivity matrix, the inversion process updates the resistivity model iteratively to minimize the objective function. This update is performed through an optimization algorithm, such as the Gauss-Newton or Levenberg-Marquardt method. Two commonly used regularization approaches were the robust inversion (L1 norm) and the smoothness-constrained inversion (L2 norm). A constraint cut off factor of 0.005 was used. The inversion continues until a satisfactory fit is achieved between the calculated and measured apparent resistivity values. Steps 2 to 6 are repeated iteratively until convergence is reached. The final inverted models were obtained, which represented the best-fitting 2D resistivity distribution that matches the field data.

3. FORWARD MODELLING

3.1 SYNTHETIC MODEL SIMULATION

In the absence of field resistivity data, the forward modeling approach is very useful to generate the resistivity response over subsurface cavities with water-filled and air-filled. Before conducting the geophysical field data acquisition, numerical modeling is initially fulfilled to choose the most suitable geo-electrical resistivity arrays to be used in ERT field data acquisition. 3 2D subsurface models were generated using Geomoto's RES2DMOD ver. 3.02.03 software, with 200 electrodes and 1m electrode spacing. The software is based on the finite element method and finite difference method which divides the subsurface into a number of rectangular meshes used to forward resistivity calculation. It analyses the apparent resistivity pseudosection for a user-defined 2-D subsurface model (Loke, 2016). The Model consists of seven different homogenous layers with distinct resistivity values. Each model has horizontal spatial coverage of 200m and a vertical extent of up to 25m. Three geological anomalies are constructed in the model such as an air-filled cavity, water-filled cavity, and dyke simulated at specific depths and distances with contrast resistivity values as shown in Fig. 2. Any air-filled void space practically has an infinite resistivity. However, RES2DMOD software does not allow infinitive resistivity value. Therefore, a resistivity value of 1,000,000Ωm has been taken to simulate similar conditions. The resistivity values for different formations have been assumed based on different published literature.

Table 1. Resistivity values of consequent homogenous layers

Model layers	Resistivity (Ωm)
Loose sand/ Alluvium	250
Sandy clay	327
Weathered sandstone	393
Sand Shale mix layer	550
Coal Seam	850
Sand Shale mix layer	550

Table 2. Resistivity values of simulated geological anomalies

Geological Anomalies	Resistivity (Ωm)
Water filled Cavity	3,5,9,15
Dyke	1190
Air-filled Cavity	1000000

3.1.1. MODEL A

The geological model A assumes only water field cavities in the coal seam. The topmost soil layer consists of 3 homogenous layers with assigned resistivities of values 250Ωm, 327Ωm, and 390Ωm. The 2nd layer is a mix of sand and shale with a resistivity value of 550Ωm. There are three water field cavities each of dimensions 19m(length)*4m(width). Within each water-filled cavity, distinct regions can be identified, each characterized by specific resistivity values of 3Ωm, 9Ωm, and 15Ωm. Beneath the coal seam, there is another sand-shale mix layer with a resistivity value of 550Ωm.

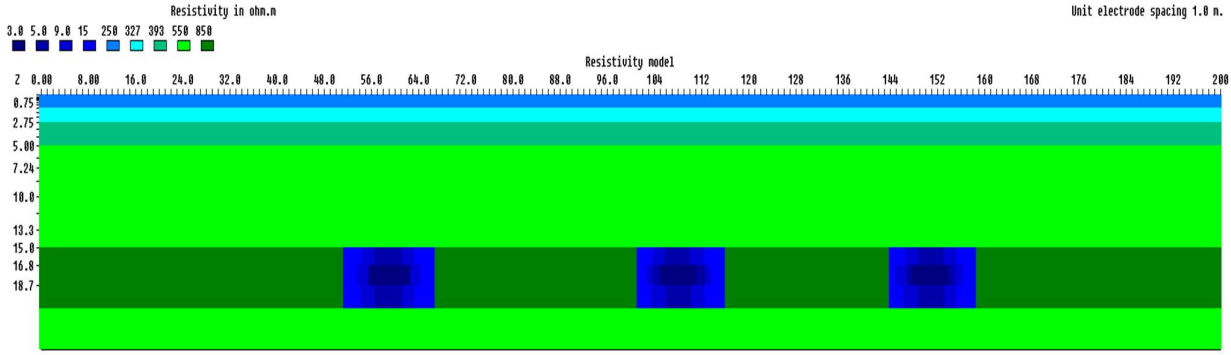

Figure 6. A simplified model of water-filled cavities in the coal seam

3.1.2. MODEL B

The geological model B consists of only airfield cavities in the coal seam. The topmost soil layer consists of 3 layers with assigned resistivities of values 250Ωm, 327Ωm, and 390Ωm. The 2nd layer is a mix of sand and shale with a resistivity value of 550Ωm. To accommodate air field cavities, which typically exhibit high resistivity values, the geological model assigns these voids with the maximum resistivity value of 1000000Ωm. There are three airfield cavities each

of dimensions 19m(length)*4m(width). Beneath the coal seam, there is another sand-shale mix layer with a resistivity value of 550Ωm.

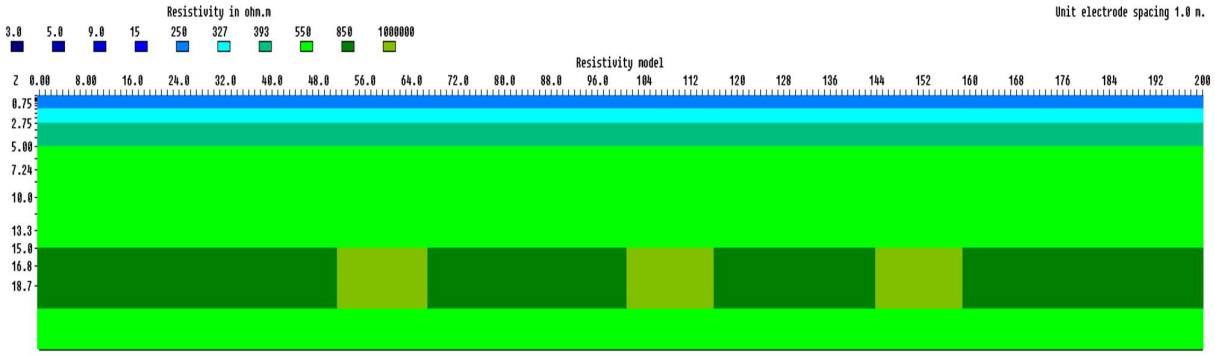

Figure 7. A simplified model of air-filled cavities in the coal seam

3.1.3. MODEL C

Model C consists of 5 layered Earth with air and water field cavities in the coal seam as well an inclined dyke. The topmost soil layer consists of 3 layers with assigned resistivities of values 250Ωm, 327Ωm, and 390Ωm. The 2nd layer is a mix of sand and shale with a resistivity value of 550Ωm. The dyke is assigned a resistivity value of 1190Ωm. The dyke is measured to be approximately 20 meters in height and 7 meters in thickness. Both cavities are of same dimensions of 19m(length)*4m(width). Beneath the coal seam, there is another sand-shale mix layer with a resistivity value of 550Ωm.

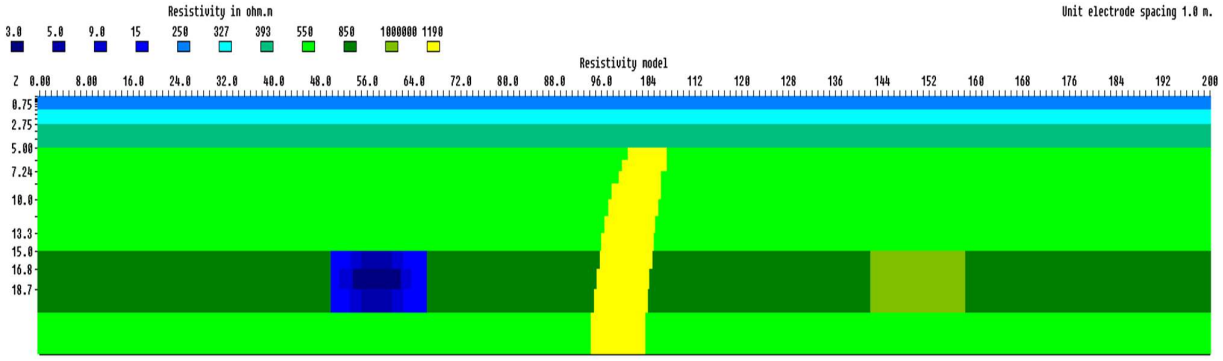

Figure 8. A model simulating water and air-filled cavities and a dyke in the coal seam

3.2 SYNTHETIC DATA

Forward modeling in RES2DMOD version 3.02 is a crucial step in the process of electrical resistivity imaging. In forward modeling, values of apparent resistivity are calculated based on current sensitivity function, the model and model parameter(resistivity). The numerical calculation methods for forward modeling of DC resistivity are mainly:

a. Integral Equations (IE) (Dieter et al., 1969; Pratt, 1972; Hohmann, 1975; Lee, 1975; Daniels, 1977; Okabe, 1981; Oppliger, 1984; Xu et al., 1988)
b. Finite element method (FD) (Coggon, 1971; Fox et al., 1980; Pridmore et al., 1981; Holcombe and Jiracek, 1984; Sasaki, 1994)
c. Finite difference method (FE) (Mufti, 1976; Dey and Morrison, 1979; Scribe, 1981; Spitzer, 1995; Zhao and Yedlin, 1996)

These methods consider the subsurface environment as a series of blocks and calculate potential values at the intersection of blocks and then calculate the apparent resistivity values for each block (Loke 2002).

3.2.1. IE METHOD

In the IE method, apparent resistivity is calculated by developing a linear relationship between model parameters, whereas resistivity modeling is non-linear. As a result, the forward modeling approach using the IE method is not well-suited for comparison with real field data due to its limitation with complex background. However, simple layered models with compact bodies, generate quicker and more accurate responses than FD (Finite Difference) and FE (Finite Element) methods (Zhdanov and Michael, 2009).

3.2.1. FD METHOD

FD Method discretizes the subsurface 2D domain into a regular grid of cells, where each point represents a resistivity value. Derivatives in the governing equations are approximated using finite differences between adjacent points. This is a simpler and more structured grid compared to FE Method. FDM is easier to implement and computationally less intensive, making it suitable for rapid calculations. However, FDM's grid structure struggles to accurately represent irregular geometries. It fails to incorporate topography variation. RES2DINV adopts the finite difference method for solving the forward modeling problem and subsequent inversion.

3.1.2. FE METHOD

FEM divides the subsurface domain into a mesh of interconnected elements, which can be triangles or quadrilaterals in 2D. Each element is described by a set of mathematical equations that approximate the behavior of resistivity in that element. These equations are derived from the governing physical equations (e.g., Poisson's equation) and take into account the resistivity values of neighboring elements. The mesh can adapt to irregular geometries, which accurately

represent complex structures. FEM involves solving a system of equations, which are computationally demanding, but it provides high accuracy and flexibility for modeling intricate subsurface variations.

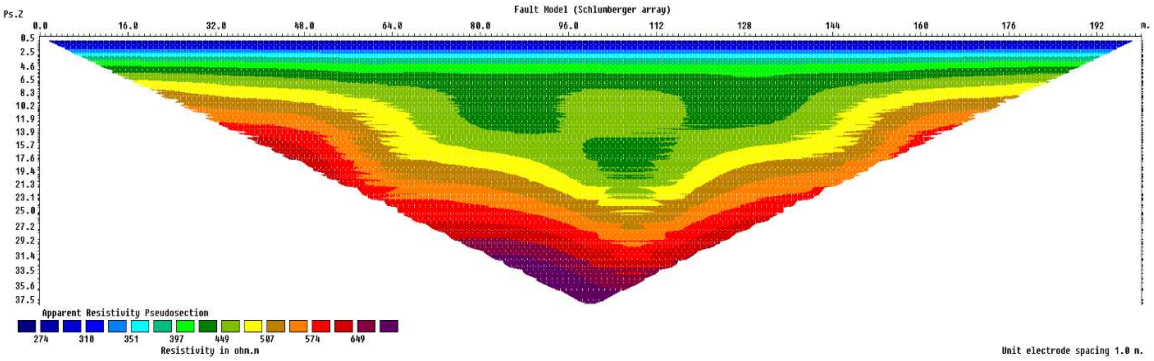

Figure 9. Apparent resistivity pseudo section generated corresponding to model A using Wenner-Schlumberger array

3.3 DAT FILE FOR RES2DINV

The forward-modeled apparent resistivity pseudo section data for each array configuration was then saved in a DAT file. 5% Gaussian noise was added to each synthetic dataset to reflect the real field scenario. This DAT file was then used as input for the Res2DInv software.

4. INVERSION

The determination of the model parameter (i.e., resistivity estimates) using the data space and model space is known as inversion. It involves mapping from data space to model space (OLDENBURG and ELLIS 1991). Inverse modeling finds a model with the most similar responses to the field data. In this study, the inversion process aims to reconstruct the subsurface resistivity distribution using measured apparent resistivity pseudo section data from forward modeling (DAT file). To carry out inversions, the commercially available RES2DINV software by GEOTOMO (2005) was used, adding 5% Gaussian noise to simulate real field conditions. The RES2DINV software employs two different inversion routines to generate 2D resistivity models from the apparent resistivity data obtained through forward modeling. The inversion routines are based on the blocky or L1-norm optimization (LOKE et al. 2003) and Gauss-Newton smoothness-constrained least-squares method for L2-norm optimization (DEGROOT-HEDLIN and CONSTABLE 1990; ELLIS and OLDENBURG 1994).

4.1. ROBUST INVERSION

This method aims to minimize the absolute difference (Abs.) between the measured and calculated apparent resistivity values. It is also known as L1 norm optimization. The L1 norm

is the objective function, defined as the sum of the absolute differences between the measured and calculated apparent resistivity values. It can be represented mathematically as:

$$\textbf{L1 norm} = \Sigma\, |\rho\_\text{calculated} - \rho\_\text{measured}|$$

ρ_calculated = calculated apparent resistivity value, ρ_measured = measured apparent resistivity values

In robust inversion we allow the number of blocks to automatically exceed the number of data points in the final inverse model resistivity section. This allows more blocks than data points, providing flexibility, noise handling, improved resolution, and non-uniqueness mitigation for realistic subsurface representations.

The cut-off factor, set at 0.05, significantly reduces measured-calculated apparent resistivity differences at any data point where it is greater than 5 percent.

The L1 norm generates blocky inverse resistivity models, suitable for models with sharp geologic boundaries, such as cavities and fracture zones. The L1 norm is robust to outliers in the data because it does not heavily penalize large differences between the measured and calculated values. Therefore, it is a better optimization choice when extreme discontinuities in the resistivity model are present.

4.2. SMOOTHNESS-CONSTRAINED LEAST SQUARES METHOD

The "smoothness constraint" is a regularization technique that is used to stabilize the inversion process by producing more geologically plausible results. This constraint is often applied in conjunction with the least squares method. The objective function is represented as:

$$\textbf{L2 norm} = \Sigma\, |\rho\_\text{calculated} - \rho\_\text{measured}|^2$$

The smoothness constraint aims to prevent unrealistic or oscillatory variations in the inverted model by penalizing rapid changes in the parameter being estimated (such as resistivity in electrical resistivity tomography). It's particularly useful in situations where the available data are insufficient to uniquely determine the subsurface structure, leading to underdetermined or ill-posed problems.

The 'Standard Gauss-Newton least-squares method, which calculates an exact solution of the least-squares equation, should be used if the number of data points and/or model cells is small (less than a few thousand). If the number of data points and/or model cells is large (more than a few thousand), the time taken to solve the least-squares equation could be the most time-consuming part of the inversion process. To reduce the inversion time, an alternative method that calculates an approximate solution of the least-squares equation using the 'Incomplete Gauss-Newton' method can be used.

4.3. INVERSION RESULTS

Three geological models were considered for 2d ERT survey and separate inversion for each array configurations were performed on each model. The inversion results are being discussed below.

4.3.1. MODEL A

Figure 11a, b, c represents inverted resistivity sections over model A corresponding to pole-dipole, dipole-dipole, and wenner-schlumberger array respectively. It is clear that the dipole-dipole inverted resistivity section in figure 11a clearly brings out water filled cavities in comparison to pole-dipole and wenner-schlumberger inverted sections. Resistivity values lesser than 64Ωm as well in the range 64-114c indicate presence of water-logged cavities. The coal layer is distorted compared to actual model and showing a resistivity variation in range 627-1106Ωm. The depth of the cavities shows very little variation compared to actual model. 3 water filled cavities can be well seen in this inverted section. In figure 11b, the pole-dipole inverted resistivity section succeeds in portraying the left and right most cavities but the middle cavity is distinct. This is due to the edge effect. Due to short vertical span of our current model, the inverted sections are being contaminated with these edge effects. This can be overcome through taking larger vertical extent. In figure 11c, the resolution of the wenner-schlumberger inverted section is very poor. This happened as the inversion became unstable at 3rd iteration due to appearance of high model resistivity value of around 72000Ωm. Apart from resolution, this inverted section succeeds in capturing S1 and S2 cavities.

Table 3. Separate array inversion results corresponding to model A

MODEL NO.	ERT Array Configurations	Maximum depth of penetration (m)	Number of iterations	RMS Error (%)	Targets detected
MODEL A	Pole-Dipole	71.2	7	1.78	S1, S3
	Dipole-Dipole	48.3	7	1.91	S1, S2, S3
	Wenner-Schlumberger	42.5	7	2.15	S1, S2

*S1, S2, S3=Consequent anomaly structures within model

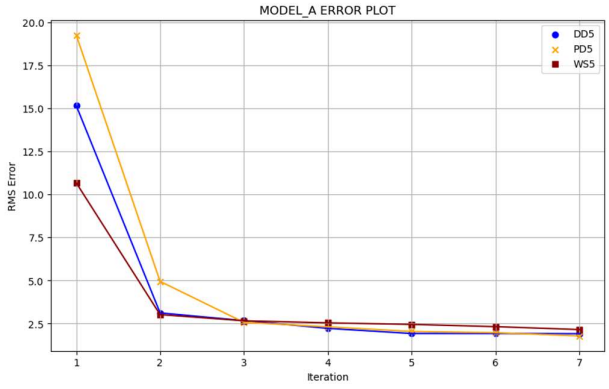

Figure 10. RMS error variation with each iteration corresponding to DD, PD and WS inverted resistivity section

MODEL A

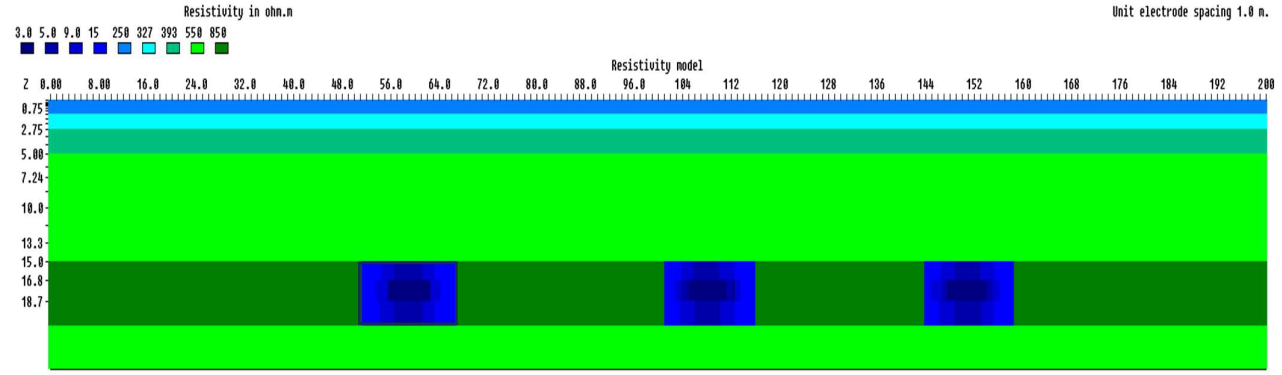

a. Dipole-Dipole Array

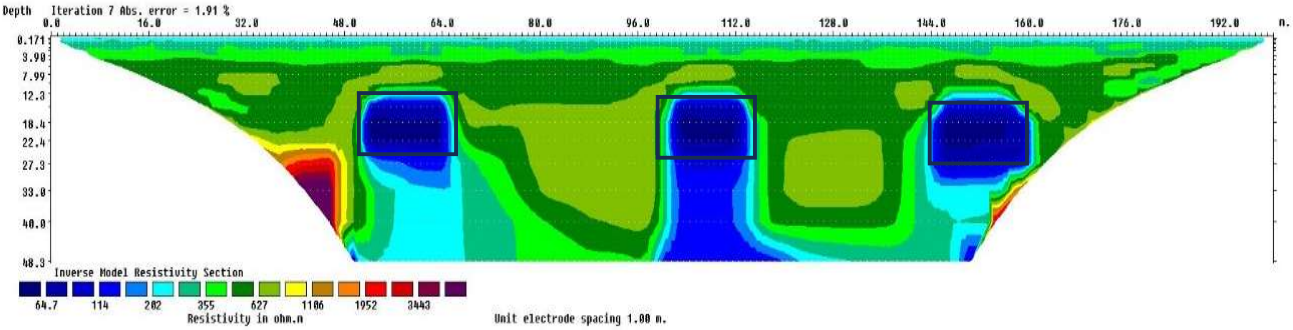

b. Pole-Dipole Array

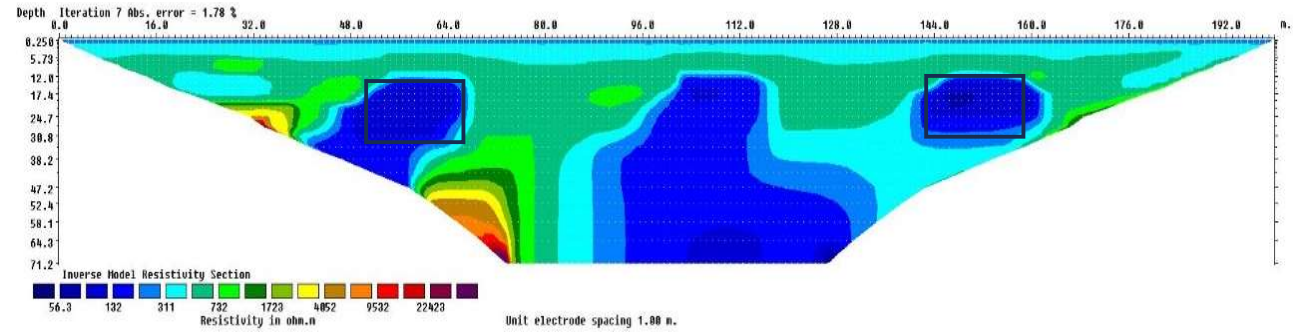

c. Wennner Schlumberger Array

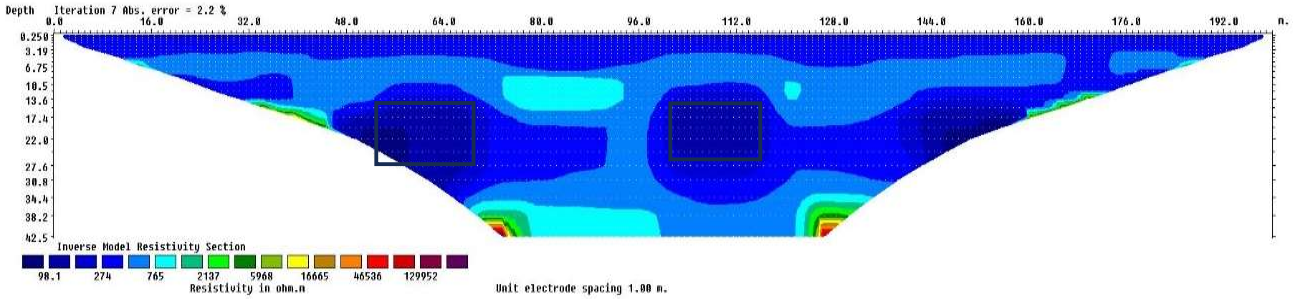

Figure 11. Inversion models of water-filled cavities in the coal seam

4.3.2. MODEL B

Figure 13a, b, c illustrates inverted resistivity sections over model B corresponding to pole-dipole, dipole-dipole, and wenner-schlumberger array respectively. The dipole-dipole inverted resistivity section in figure 13a clearly brings out air filled cavities in comparison to pole-dipole and wenner-schlumberger inverted sections. Resistivity values bigger than 3000Ωm represent presence of air-filled cavities. The coal layer is distorted compared to actual model and showing a resistivity variation in range 665-999Ωm. The depth of the cavities shows very little variation compared to actual model. 3 water filled cavities can be well seen in this inverted section. The S2 and S3 anomaly are being engulfed by the edge effect hence are poorly resolved compared to S1. In figure 13b, the pole-dipole inverted resistivity section succeeds in portraying the middle and right most cavities (S2 and S3) but the middle cavity is more distinct. High resistivity area more than 3413Ωm indicate presence of cavities. The S1 cavity is left unresolved but clearly indicates presence of high resistivity anomalous zone. In figure 13c, the resolution of the wenner-schlumberger inverted section is very poor. Although the inverted section indicates the presence of anomalous zones as vertical sections but fails to delineate the cavities.

Table 4. Separate array inversion results corresponding to model A

MODEL NO.	ERT Array Configurations	Maximum depth of penetration (m)	Number of iterations	RMS Error (%)	Targets detected
MODEL B	Pole-Dipole	70.9	6	1.77	S2, S3
	Dipole-Dipole	48.3	6	1.72	S1, S2, S3
	Wenner-Schlumberger	39.9	6	1.71	None

*S1, S2, S3=Consequent anomaly structures within model

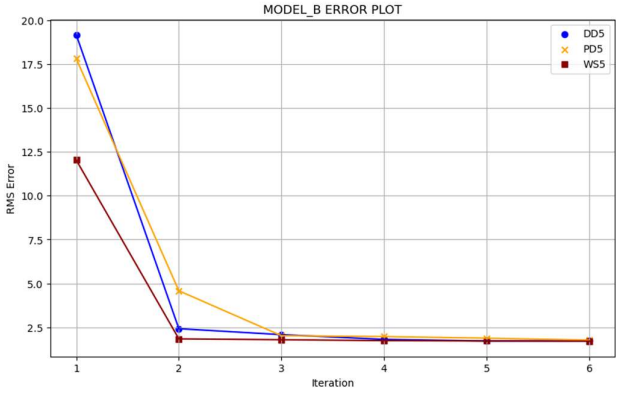

Figure 12. RMS error variation with each iteration corresponding to DD, PD and WS inverted resistivity section

MODEL B

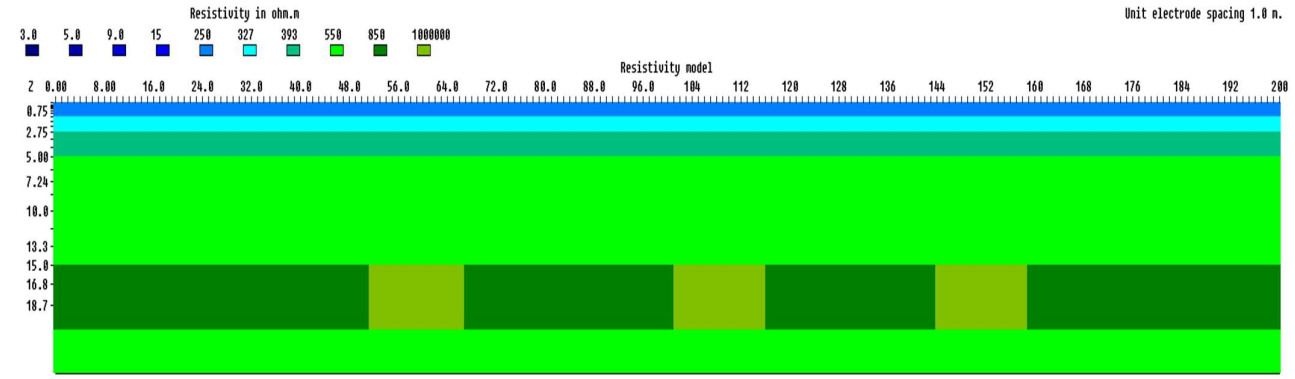

a. Dipole-Dipole Array

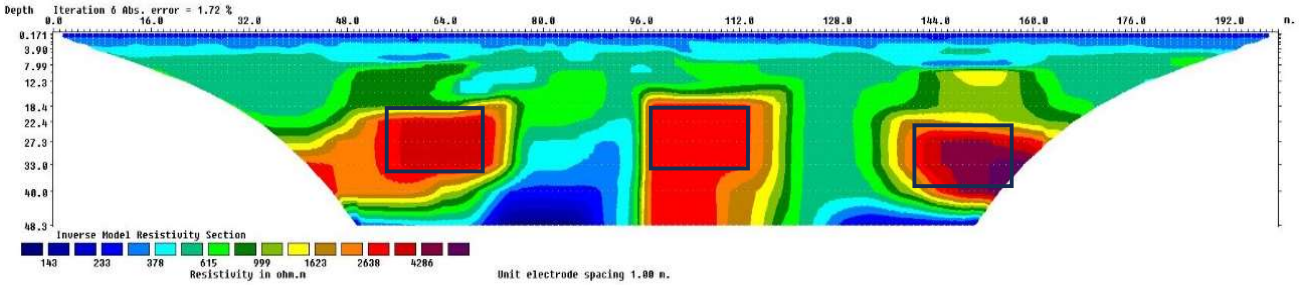

b. Pole-Dipole Array

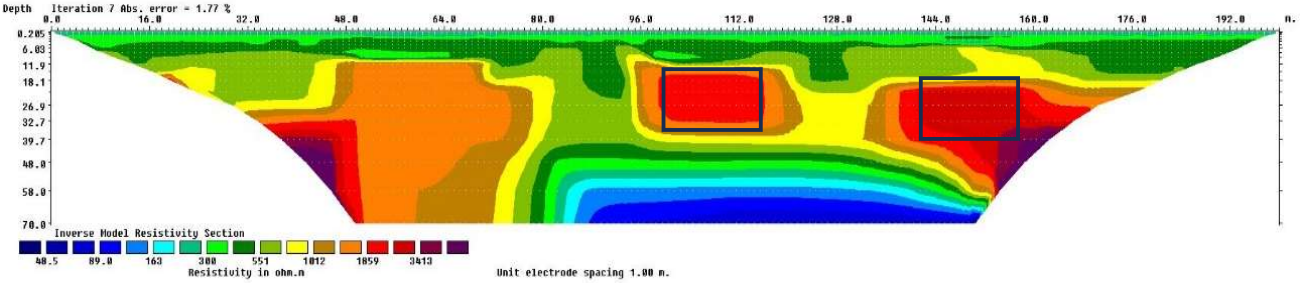

c. Wennner Schlumberger Array

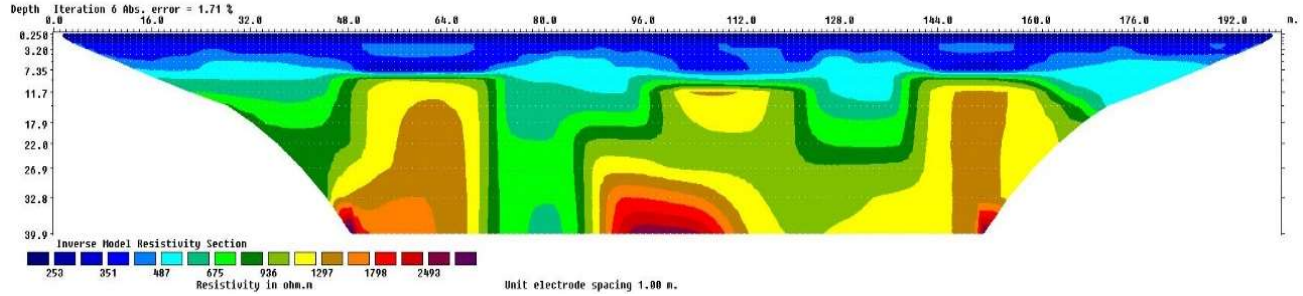

Figure 13. inversion models of air-filled cavities in the coal sea

4.3.3. MODEL C

Figure 15a, b, c illustrates inverted resistivity sections over model C corresponding to pole-dipole, dipole-dipole, and wenner-schlumberger array respectively. The corresponding actual geological model consists of a water filled cavity (S1), a dyke (S2) and an air-filled cavity (S3). The dipole-dipole inverted resistivity section in figure 15a clearly resolves S1 and S2 anomalies in comparison to pole-dipole and wenner-schlumberger inverted sections. Resistivity values around 1095Ωm represent the location of dyke, which is close to actual resistivity value in initial model C. The shape of the dyke is not clearly resolved at the bottom side. Resistivity value lesser than 64Ωm represent presence of water-logged cavities. The coal layer is distorted compared to actual model and showing a resistivity variation in range 609-1095Ωm. The depth of the cavities is showing very large variation compared to actual model. The S3 anomaly is being engulfed by the edge effect hence is poorly resolved. In figure 13b, the pole-dipole inverted resistivity section only resolves the left most cavity (S1) and the other anomalies are completely undetectable. In figure 13c, the resolution of the wenner-schlumberger inverted section is very poor compared to that of pole-dipole and dipole-dipole inverted sections despite it has the capability to resolve lateral structures. Although the inverted section indicates the presence of anomalous zones as vertical sections but fails to delineate the anomalies.

Table 5. Separate array inversion results corresponding to model A

MODEL NO.	ERT Array Configurations	Maximum depth of penetration (m)	Number of iterations	RMS Error (%)	Targets detected
MODEL C	Pole-Dipole	70.9	6	2.16	S1, S3
	Dipole-Dipole	48.3	6	1.80	S1, S2,S3
	Wenner-Schlumberger	39.9	6	1.73	S1, S3

*S1, S2, S3=Consequent anomaly structures within model

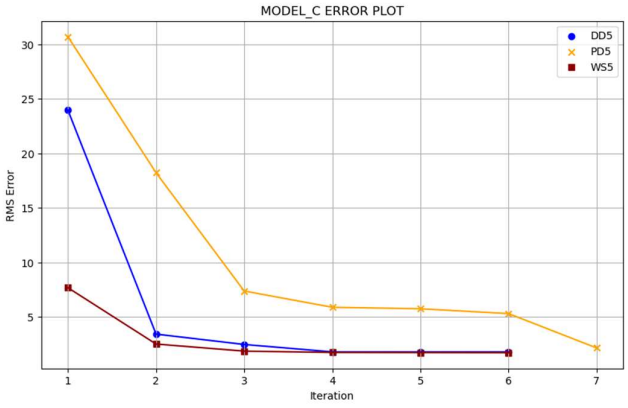

Figure 14. RMS error variation with each iteration corresponding to DD, PD and WS inverted resistivity section

MODEL C

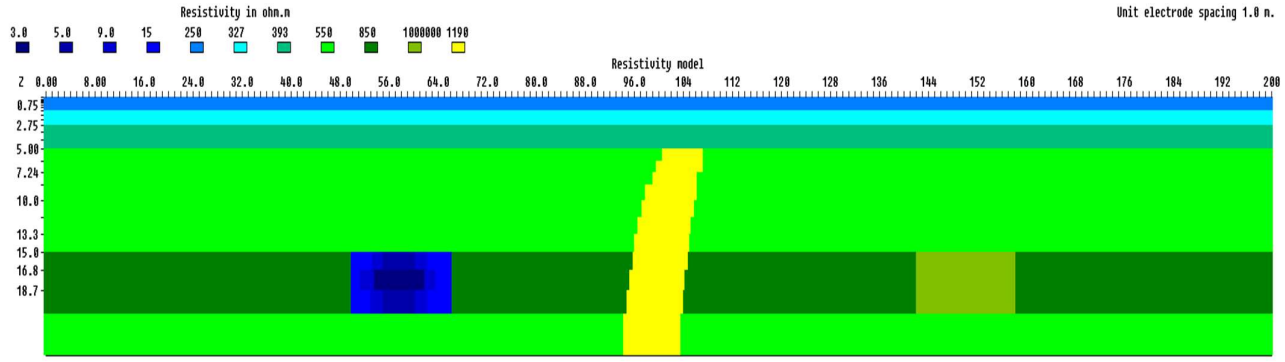

a. Dipole-Dipole Array

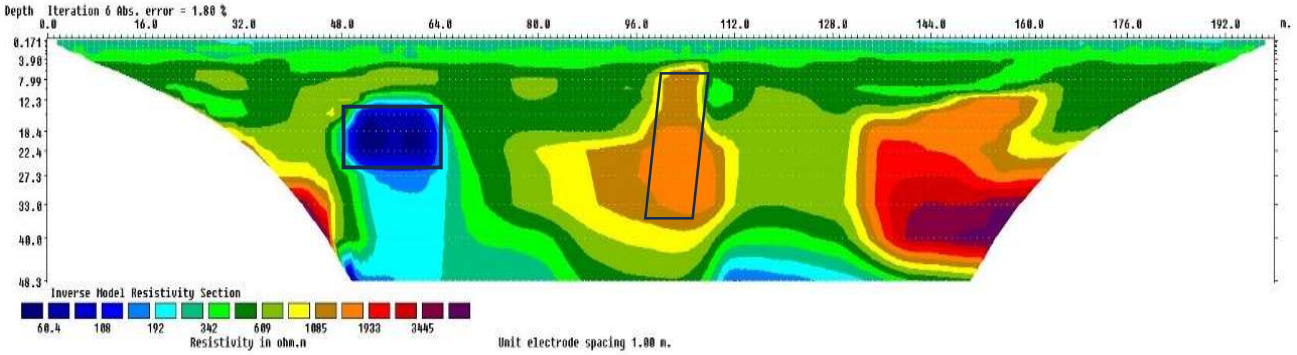

b. Pole-Dipole Array

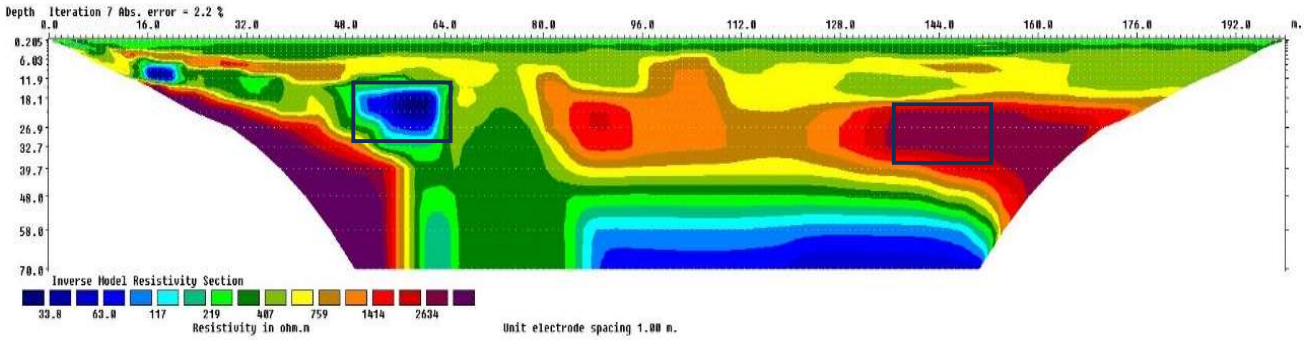

c. Wennner Schlumberger Array

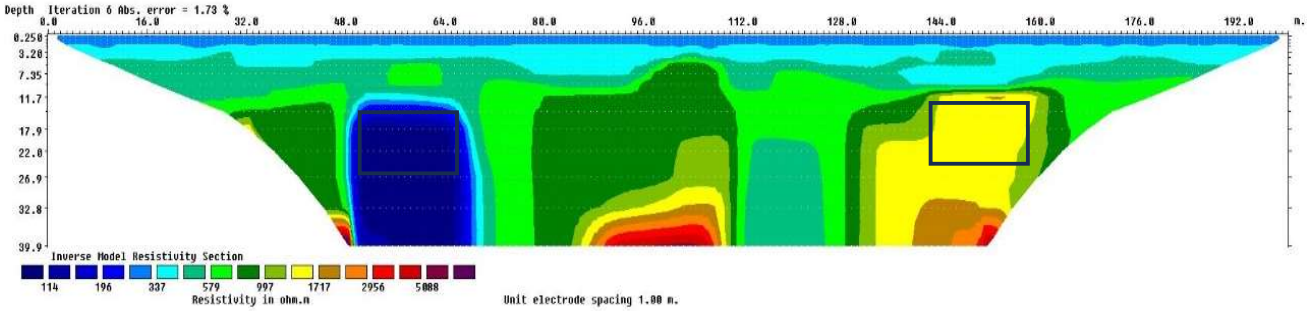

Figure 15. inversion modelss of air-filled, dyke and water-filled cavities in the coal seam

5. DATA LEVEL SYNTHESIZATION (DLS) METHOD

Data Levels Synthesization (DLS) method is the process of merging the data levels of two or more different optimized geoelectrical apparent resistivity arrays data (DAT file) into one final resistivity image to achieve high-resolution 2D apparent resistivity pseudosection (Lee et al., 2018). It is also preferred as Joint Inversion. At the end of the numerical modeling phase, three distinct optimized arrays were chosen to be applied in ERT field data acquisition. The possible combination of all three selected types of geoelectrical resistivity arrays are D-D + WS, PD + WS and D-D + P-D + WS. The final data levels arrangement for these three possible combinations of three different arrays using DLS method is shown in Fig. 17, 19, 21 respectively. Table 6 shows an example of W-S + D-D raw data file in general array format. This raw data file is made up of a total 39525 data points resulted from the combination of data points from W-S array (18285 data points) and D-D array (21240 data points). This 'W-S + D-D.DAT' file is then inputted into RES2DINV program to perform inversion to generate inversed model. The final resistivity image produced from the merged resistivity data from both arrays are used to access the effectiveness of DLS method to produce high resolution 2-D ERT imaging.

Table 6. Example of W-S + D-D raw data file in general array format.

DD + WS DAT file	Comments
Cavity model	Name of survey line
1.0	Unit electrode spacing
11	Type of array (111 for general array)
0	Type of sub-array (0 for non-specific)
Type of measurement (0 = apparent resistivity, 1 = resistance)	Header
0	0 indicates apparent resistivity
39525	Number of data points
1	Type of x-location, 0 for true horizontal distance
0	Flag for I.P. data, 0 for none (1 if present)
4 1.0000,0.0 0.0000,0.0 2.0000,0.0 3.0000,0.0 255.80447	The format for each data point is:
4 2.0000,0.0 1.0000,0.0 3.0000,0.0 4.0000,0.0 255.75537	x- and z-location of C1, C2, P1, P2,
4 3.0000,0.0 2.0000,0.0 4.0000,0.0 5.0000,0.0 255.74434	Number of electrodes used,
4 4.0000,0.0 3.0000,0.0 5.0000,0.0 6.0000,0.0 255.74019	Apparent resistivity or resistance value
…	
…	Same format for other data points
…	
4 2.0000,0.0 200.0000,0.0 92.0000,0.0 110.0000,0.0 736.77283	Last data point
0,0,0,0,0	Ends with a few zeros.

5.1. DLS INVERSION RESULTS

5.1.1. MODEL A

Figure 17a, b, c represents joint inverted resistivity sections over model A corresponding to PD +WS, DD + WS, and PD + DD + WS respectively. It is clear that the PD+WS inverted resistivity section in figure 17a fails to brings out clear water filled cavities in comparison to DD + WS, and PD + DD + WS inverted sections. Resistivity values lesser than 64Ωm as well in the range 32Ωm indicate presence of water-logged cavities. The coal layer is distorted compared to actual model and showing a resistivity variation in range 963Ωm. The depth of the cavities shows very little variation compared to actual model. 2 water filled cavities can be well seen in this inverted section but the shapes are poorly resolved. In figure 17b, DD + WS inverted resistivity section succeeds in portraying the three cavities but the S1 and S2 anomalies are more distinct. Due to the edge effect, S3 is poorly resolved. Due to short vertical span of our current model, the inverted sections are being contaminated with these edge effects. In figure 17c, the resolution of the PD + DD + WS inverted section is very close to initial model. The PD + DD + WS inverted section proves to be the most efficient representation of the subsurface model as it captures the rectangular shapes of cavities without much deteoriation.

Table 7. joint inversion results corresponding to model A

MODEL NO.	JOINT INVERSION	Maximum depth of penetration (m)	Number of iterations	RMS Error (%)	Targets detected
MODEL A	DD + WS	47.9	3	7.98	S1, S2
	PD + WS	73.4	3	2.67	S1, S2, S3
	DD + PD + WS	71.2	7	0.51	S1, S2, S3

*S1, S2, S3=Consequent anomaly structures within model

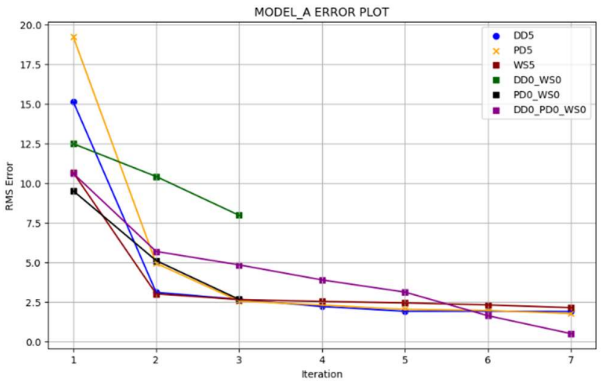

Figure 16. RMS error variation with each iteration corresponding to both separated and joint inverted resistivity section

MODEL A

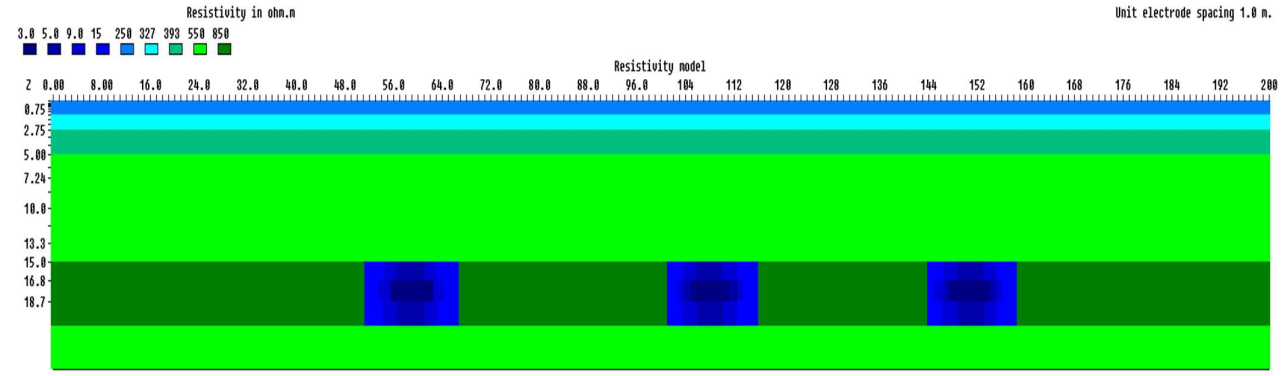

a. Dipole-Dipole + Wenner-Schlumberger Array

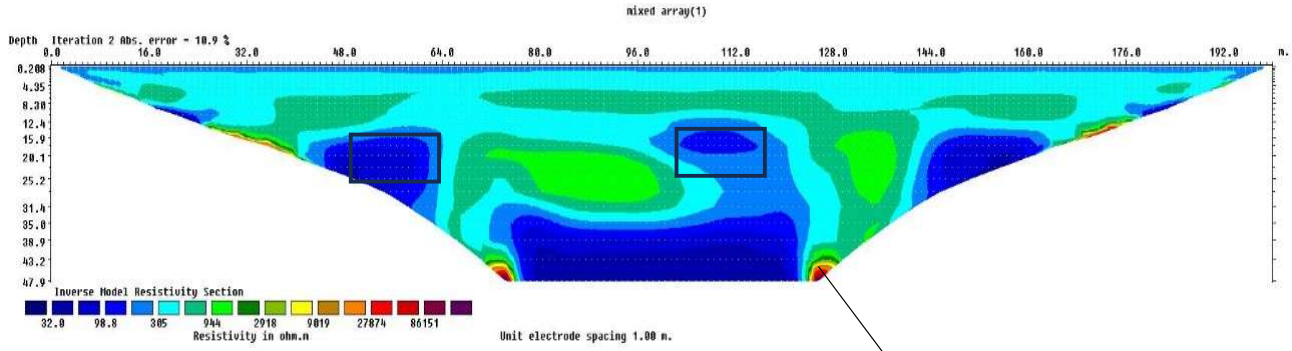

b. Pole-Dipole + Wenner-Schlumberger Array

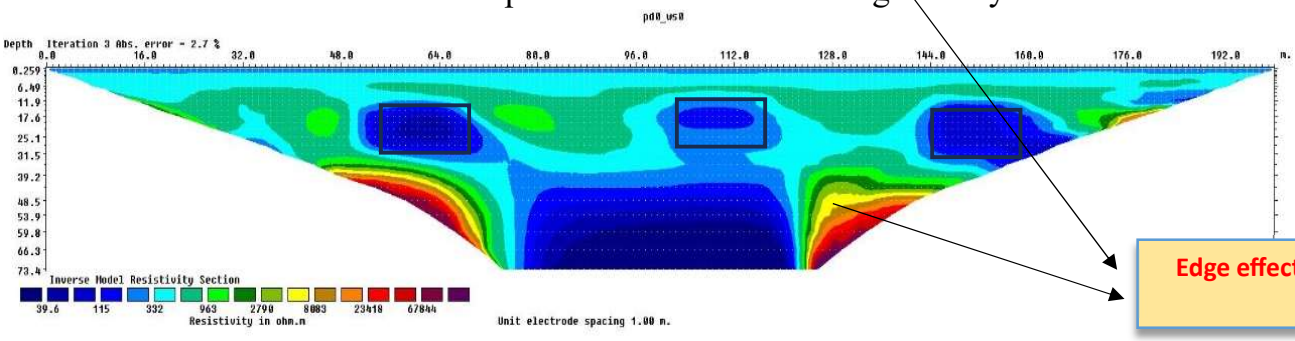

Edge effects

c. Pole-Dipole + Dipole-Dipole + Wenner-Schlumberger Array

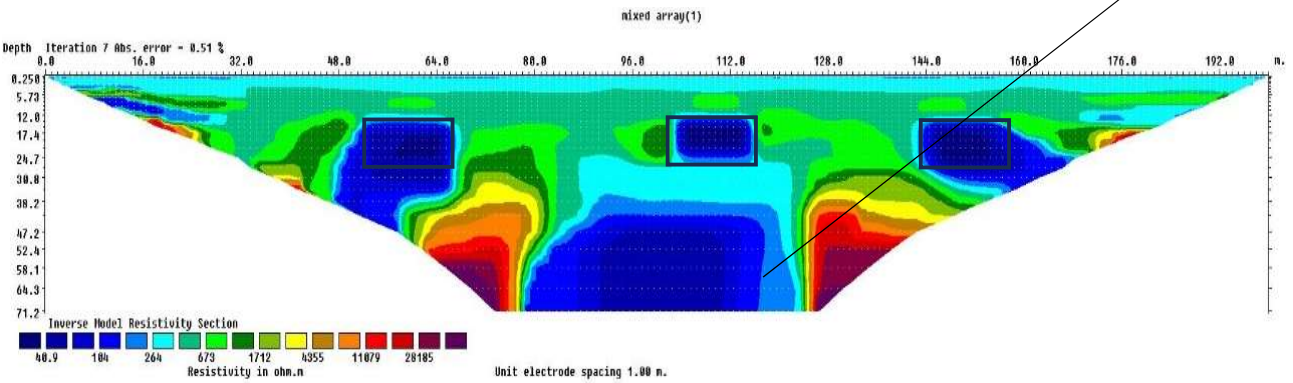

Figure 17. Joint inversion models of water-filled cavities in the coal seam

5.1.2. MODEL B

Figure 19a, b, c represents joint inverted resistivity sections over model A corresponding to PD +WS, DD + WS, and PD + DD + WS respectively. It is clear that the PD+WS inverted resistivity section in figure 19a fails to brings out clear air-filled cavities in comparison to DD + WS, and PD + DD + WS inverted sections. It happened as the RMS error kept on increasing and maintained values above 13%. Resistivity values bigger than 4000Ωm indicate presence of air-filled cavities. The coal layer is distorted compared to actual model and showing a resistivity variation in range 900Ωm. The depth of the cavities shows huge variation compared to actual model. One air-filled cavity can be well seen in this inverted section but the shapes are poorly resolved. In figure 19b, DD + WS inverted resistivity section succeeds in portraying one cavity as well but the shape is more distinct. Due to the edge effect, S1 andS3 are poorly resolved. Due to short vertical span of our current model, the inverted sections are being contaminated with these edge effects. In figure 19c, the resolution of the PD + DD + WS inverted section is very close to initial model. The PD + DD + WS inverted section in figure 19c fails to provide satisfactory output. It happened as the inversion became unstable in the 4th iteration indicating a high resistivity value of 1808380Ωm for the first model block at 28th level. Somehow, it succeeded resolving the S2 cavity though the shape was poorly retained.

Table 8. joint inversion results corresponding to model A

MODEL NO.	JOINT INVERSION	Maximum depth of penetration (m)	Number of iterations	RMS Error (%)	Targets detected
MODEL B	DD + WS	47.9	7	16.88	S2
	PD + WS	73.4	7	2.72	S2
	DD + PD + WS	72.1	2	14.72	S1, S2

*S1, S2, S3=Consequent anomaly structures within model

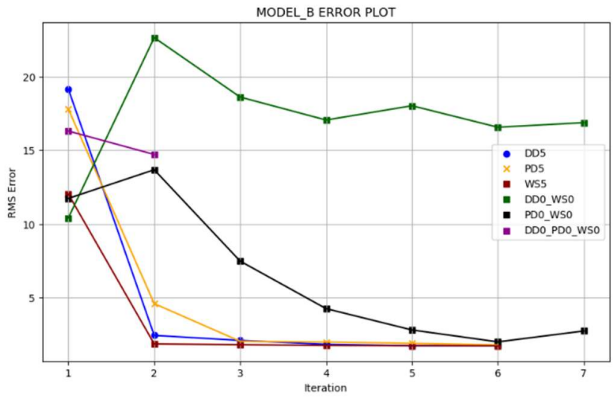

Figure 16. RMS error variation with each iteration corresponding to both separated and joint inverted resistivity section

MODEL B

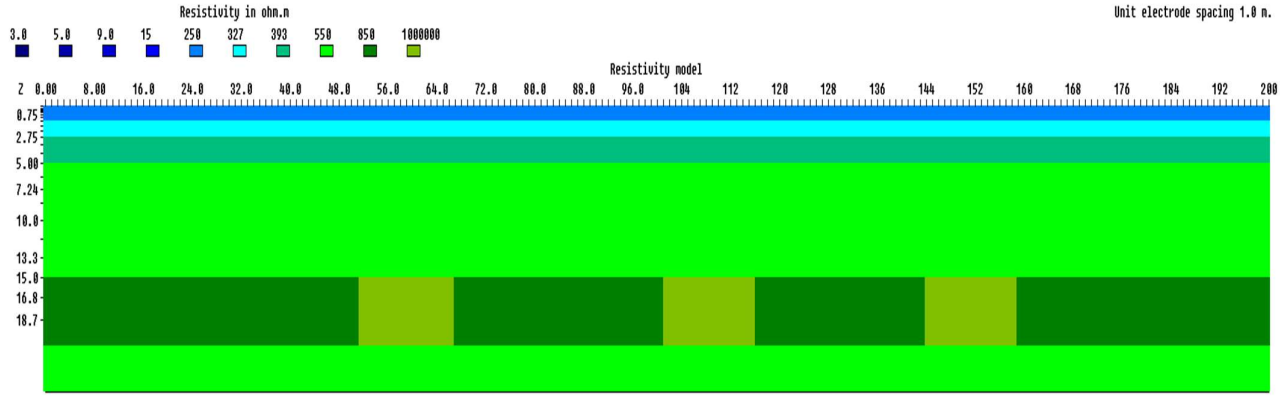

a. Dipole-Dipole + Wenner-Schlumberger Array

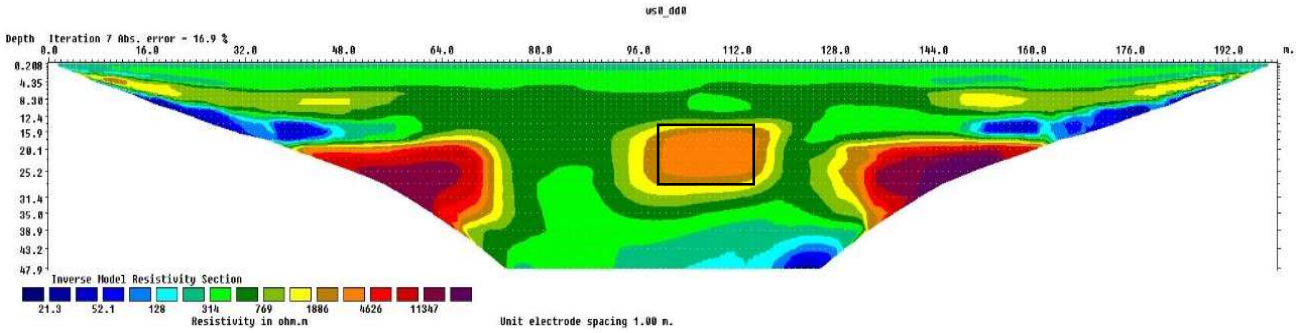

b. Pole-Dipole + Wenner-Schlumberger Array

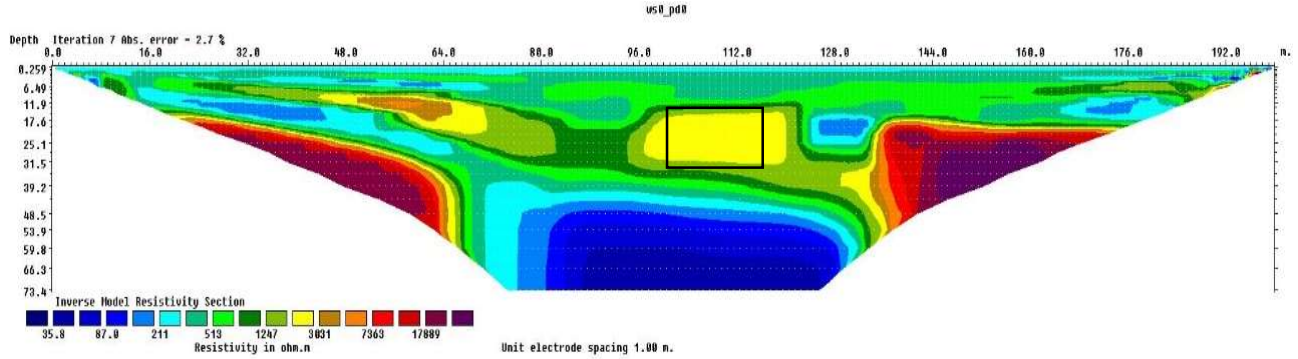

c. Pole-Dipole + Dipole-Dipole + Wenner-Schlumberger Array

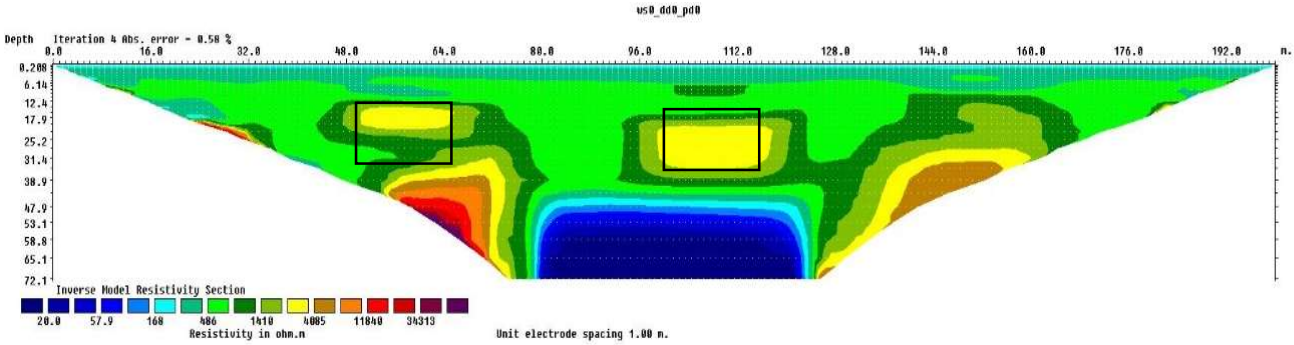

Figure 19. Joint inversion models of air-filled cavities in the coal seam

5.1.2. MODEL C

Figure 21a, b, c represents joint inverted resistivity sections over model A corresponding to PD +WS, DD + WS, and PD + DD + WS respectively. It is clear that the PD+WS inverted resistivity section in figure 21a fails to brings out clear air-filled cavities in comparison to DD + WS, and PD + DD + WS inverted sections. Resistivity values in range 9-27Ωm indicate presence of water-filled cavity. The coal layer is distorted compared to actual model and showing a resistivity variation in range 900Ωm. The depth of the cavities shows huge variation compared to actual model. One water-filled cavity can be well seen in this inverted section but the shapes are poorly resolved. Though the dyke is not properly detected, but the shape is retained to some extent. In figure 21b, DD + WS inverted resistivity section illustrates poor resolution in portraying dyke as well air-filled cavity. Due to the edge effect, S2 andS3 are poorly resolved. The shape of water filled cavity is also poor compared to separate DD array. In figure 21c, the resolution of the PD + DD + WS inverted section is comparatively close to initial model. Although, the PD + DD + WS inverted section in figure 21c fails to capture S3 but the vertical dyke is clearly captured. The edge effects are very prominent in each joint inverted model compared to separated array output.

Table 9. joint inversion results corresponding to model A

MODEL NO.	JOINT INVERSION	Maximum depth of penetration (m)	Number of iterations	RMS Error (%)	Targets detected
MODEL C	DD + WS	47.9	7	5.80	S1, S2
	PD + WS	73.4	7	5.61	S1
	DD + PD + WS	72.1	8	0.18	S2, S3

*S1, S2, S3=Consequent anomaly structures within model

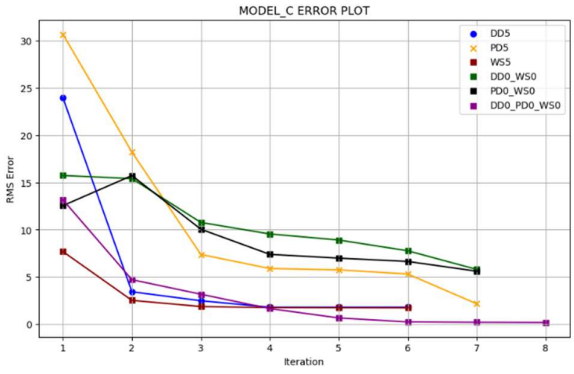

Figure 16. RMS error variation with each iteration corresponding to both separated and joint inverted resistivity section

MODEL C

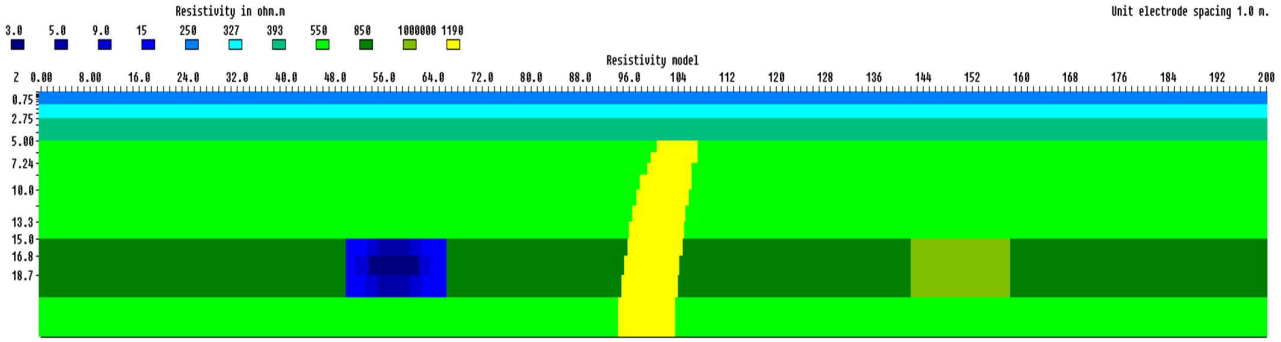

a. Dipole-Dipole + Wenner-Schlumberger Array

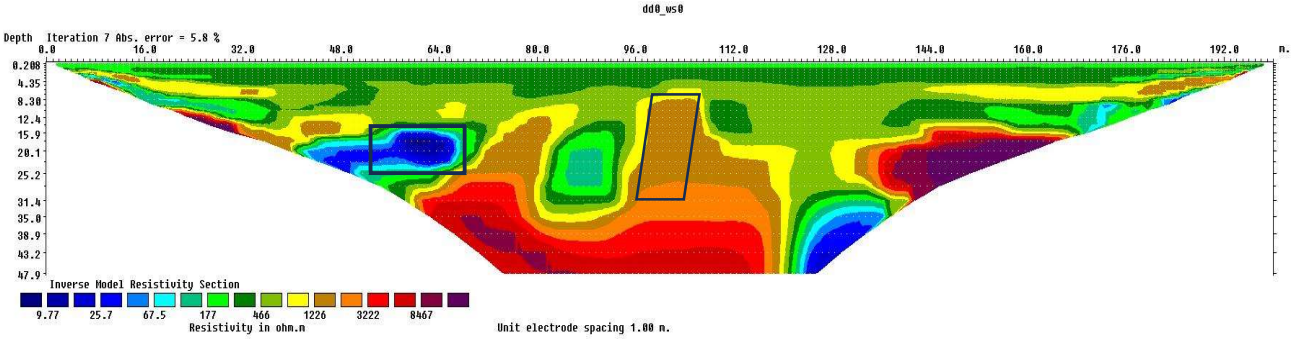

b. Pole-Dipole + Wenner-Schlumberger Array

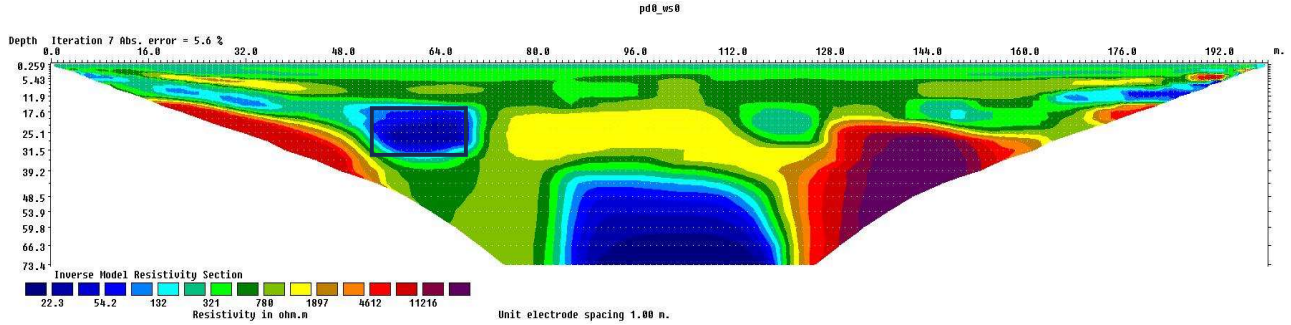

c. Pole-Dipole + Dipole-Dipole + Wenner-Schlumberger Array

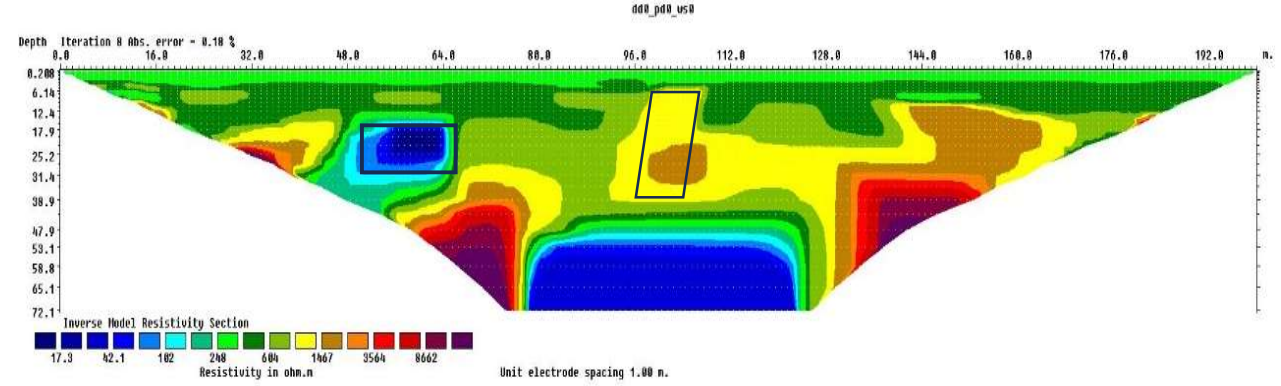

Figure 21. Joint inversion models of water-filled, air-filled cavities and a dyke in the coal seam

6. CONCLUSION

1. In separate ERT survey for pole-dipole, dipole-dipole, wenner-schlumberger array, the best performing array was found to be dipole-dipole array. Dipole-dipole array was able to detect S1, S2, S3 anomalies properly in model A and model B. It even detected the dyke with better resolution compared to other arrays in model C. But it failed to detect the S3 anomaly in the model C due to edge effect.

2.The performance of pole-dipole array was next to dipole-dipole array. It was able to delineate S1 and S3 anomalies in the consequent model A and model C. Due to edge effect, it could not detect S1 anomaly in model B. It also failed to delineate the dyke in model C. The penetration depth was the highest for this configuration. It is a suitable option to delineate lateral variation taking place at deeper depths.

3.The Wenner-schlumberger array failed drastically to delineate most of the anomalies. Most of the time, it led to failure of inversion as higher resistivity values were assigned to model blocks.

4. Each inversion model was affected by edge effects. This can be overcome if we consider geological models with higher depth of penetration than the pseudo depth of data points.

5.Joint inversion models were though provided interesting results, but due to edge effects some of the models failed in proper delineation of anomalies.

6.Joint inversion models provided more accurate shape delineation than individual array inversion model.

7.The joint inversion result of PD and WS as well DD and WS in model C provided even poorer resolution than individual array. Joint inversion is though a suitable choice, but can interpret wrong information as Synthesization of output data of two or more array leads to a noisy data. Before inversion, corresponding noisy data points should be removed for much accurate shape delineation.

8.The joint inversion of DD, PD and W generated astounding result in model A and model C. In model A, the water cavities shape and size were accurately delineated with a convergence value for the rms error of 0.51%. In model C, the upper portion of the dyke was well delineated compared to other configurations.

REFERENCES

1. Hasan, Muhammad, et al. "Application of VES and ERT for delineation of fresh-saline interface in alluvial aquifers of Lower Bari Doab, Pakistan." *Journal of Applied Geophysics* 164 (2019): 200-213.

2. Loke MH, Barker RD (1996a) Rapid least-squares inversion of apparent resistivity pseudosections by a quasi-Newton method. Geophysics Prospect44:131–152. doi:10.1111/j.1365-2478.1996. tb00142.x

3. Varfinezhad, Ramin, and Behrooz Oskooi. "2D DC resistivity forward modeling based on the integral equation method and a comparison with the RES2DMOD results." *Journal of the Earth and Space Physics* 45.4 (2020): 43.

4. Varfinezhad R, Oskooi B. 2D DC resistivity forward modeling based on the integral equation method and a comparison with the RES2DMOD results. Journal of the Earth and Space Physics. 2020 Jan 21;45(4):43.

5. Zhdanov, Michael S. *Geophysical electromagnetic theory and methods*. Elsevier, 2009.

6. Ishola, K. S., M. N. M. Nawawi, and K. Abdullah. "Combining multiple electrode arrays for two-dimensional electrical resistivity imaging using the unsupervised classification technique." *Pure and Applied Geophysics* 172 (2015): 1615-1642.

7. Szalai, Sándor, Attila Novák, and László Szarka. "Depth of investigation and vertical resolution of surface geoelectric arrays." *Journal of Environmental & Engineering Geophysics* 14.1 (2009): 15-23.

8. Dahlin, Torleif, and Bing Zhou. "A numerical comparison of 2D resistivity imaging with 10 electrode arrays." *Geophysical prospecting* 52.5 (2004): 379-398.

9. Loke, M. H. "Topographic modelling in electrical imaging inversion." *EAGE 62nd Conf. Tech. Exhib. Glas. Scotland*. 2000.